

Analytical aeroacoustic model for coaxial rotors in Urban Air Vehicles

David Oort Alonso*

In the envisioned future of Urban Air Mobility (UAM), compact, autonomous, vertical-takeoff-and-landing, electric (eVTOL) aircraft will populate the hearts of cities. It has been found that noise requirements cannot easily be met, even with generous long-term technological assumptions. This paper presents a new formulation of conventional Blade Element & Momentum Theory (BEMT) for coaxial rotors in non-axial flow coupled with Hanson's aeroacoustic analogy. The implemented numerical tool offers a tremendous speed advantage over time-stepping methods such as Free-wake and Computational Fluid Dynamics (CFD) approaches and therefore allows for rotor acoustic design optimization at the conceptual design stage.

Nomenclature

Nomenclature	
α	Angle of attack, rad
λ	Non-dimensional flow velocity
μ	Advance ratio, $= V_T / (\Omega R)$
Ω	Rotational speed, rad/s
ϕ	Inflow angle, rad
ψ	Rotor azimuth angle, rad
ρ	Air density, kg/m ³
σ	Rotor solidity
θ	Blade pitch, rad
A	Area, m ²
a	Non-dimensional radial contraction of upper rotor wake
a_∞	Speed of sound, m/s
B	Blade number
B_D	Chord-to-diameter ratio
c	Blade chord, m
C_d	Drag coefficient
C_l	Lift coefficient
C_P	Rotor power coefficient, $= P / \pi \rho \Omega^3 R^5$
C_Q	Rotor thrust coefficient, $= T / \pi \rho \Omega^2 R^5$
C_T	Rotor thrust coefficient, $= Q / \pi \rho \Omega^2 R^4$
C_{lk}, C_{dk}	k th lift/drag harmonic coefficient
d_o, ψ_o, θ_o	Observer-rotor distance and angles
F	Prandtl tip loss function
f	Exponent in Prandtl tip-loss function
h	Inter-rotor vertical distance, m
$J_x(\square)$	Bessel function of the first kind of order x and argument \square
k	Order of load harmonic
M	Mach number
m	Sound harmonic
P	Rotor power, W
Q	Rotor torque, Nm
R	Rotor radius, m
r	Normalized radial position, y/R
T	Rotor thrust, N
V	Free-stream velocity, m/s
v	Induced velocity, m/s
y	Radial position, m
Subscripts	
\square_0	Quantity in zero-lift conditions
\square_l	Property of the lower rotor
\square_o	Property of the observer
\square_P	Axial flow component
\square_s	Quantity in stalled conditions
\square_T	Tangential flow component
\square_u	Property of the upper rotor
Conventions	
$d\square$	Discretized quantity, incremental amount
i	Imaginary number

*Bachelor Honours Student, Faculty of Aerospace Engineering, Delft University of Technology

I. Introduction

A. Urban Air Mobility

Urban Air Mobility (UAM) is a conceived air taxi service. It is realized by compact electric flying vehicles that can fit 1-5 passengers, take-off and land vertically (eVTOL) and can fly approximately 300 km at speeds much higher than conventional helicopters through an uncongested atmosphere. Such a system has several advantages over existing transport methods:^{1,2}

- Greatly reduced commute times and/or greatly increased Mobility Reach (accessible land area with a given commute time³), by avoiding gridlock
- No infrastructure (highways, railways, tunnels, tubes) needed between destinations, only landing pads are needed.
- Lower energy costs, due to efficient electric propulsion systems¹
- Lower (or no) pilot operating costs, due to autonomy¹

Since the first powered flight in 1903, flying machines have been notoriously noisy. For this reason, airports are usually built on the outskirts of cities, and airspace restrictions keep helicopters and jets at high altitudes when flying over populated areas. In the envisaged future of UAM, these flying vehicles will continuously take-off and land from city centers. In a whitepaper published by Uber in 2016, their vision for an on-demand aviation service is outlined and called “Uber Elevate”.² A significant portion of the Uber Elevate paper is devoted to defining a set of quantitative noise goals. They eventually select a target noise level of 62 dBA (A-weighted decibels) with the vehicle hovering 150 m overhead.

It was found by Brown et al.¹ in 2018 that “the 62-dBA noise requirement is not met, even with the most generous long-term technological assumptions”. Noise pollution, therefore, is one of the greatest barriers of the UAM market.

Brown et al.¹ note that “while some noise benefits can be obtained merely by replacing the rotors, larger benefits are possible if the aircraft is redesigned with noise as a primary concern”. This stresses the need for a multi-disciplinary optimization framework that can be used at a conceptual level of vehicle design, and thus must be highly parametric, and fast to run. The benefits of such an optimization framework are not only beneficial to the air taxis that embody the on-demand aviation service but to a much broader class of next-generation flying vehicles such as UAVs and heavy-lift delivery drones that might also have stringent noise requirements.

In the advent of these heavy-lift, eVTOL and ultra-compact designs, coaxial rotors are becoming a fitting design choice. [Figure 1](#) shows some examples of conceived and existing air taxi concepts making use of coaxial rotors. This configuration has several advantages over its counterpart, the single rotor^{4,5}

- They are superior in efficiency for the same area, thanks in part to the positive swirl recovery effect. Helicopters with coaxial rotors will usually have greater payload carrying capabilities.⁶ In other words, for the same payload, helicopters using coaxial rotors tend to be more compact (with a smaller footprint on the ground). It should be noted that, due to the flow interaction between the two rotors, a coaxial-rotor produces less thrust than the sum of thrust produced by two single rotors. Leishman⁷ has analytically showed that the coaxial-rotor requires approximately 22% more power to produce the same thrust of two separated single rotors combined. However, in a field like UAM or delivery drones, compactness of the design is a serious driver which makes the use of coaxial rotors appealing.
- No net torque on the supporting structure due to oppositely spinning rotors.
- Lower rotational speed of individual rotors allows the coaxial system to be able to operate at higher forward tangential speeds without reaching drag divergence at the advancing blade tips.

Most of the disadvantages of coaxial rotors are related to the mechanical complexity of the swash plate system at the rotor hub.⁵ This is why in the past their use was quite limited in comparison to single rotors. However, Distributed Electric Propulsion (DEP) has made coaxial drives much easier in most cases requiring less articulation, less gearboxes, etc.



Figure 1: Coaxial rotors used in passenger drones, personal flying devices and helicopters. All rotors operated at high incidence angles in forward flight (non-axial flow conditions).

B. Coaxial Rotor Aeroacoustic modelling

Generally, the aeroacoustic modelling problem is split up into compatible aerodynamic and acoustic modelling methods; aeroacoustics fundamentally deals with aerodynamically generated sound. This section reviews on a high-level the different approaches that have been tried to model the aerodynamic performance of coaxial rotors and a few acoustic analogies that were considered to model the sound generated by the aerodynamic interactions of both rotors.

1. Aerodynamic Performance of Coaxial Rotors

While the analysis of single propellers dates back to the 19th century, with Rankine⁸ developing momentum theory for marine propulsion, it was only in the 1950's that Harrington⁹ modelled coaxial rotors using hovering-performance theory. "Simple but reasonably good mathematical models have previously been developed for prediction of thrust in single rotor helicopters, but few models have been developed for thrust prediction of coaxial-rotors".⁶ Leishman, who has extensively studied the performance of coaxial rotors, has published several papers on the topic.¹⁰⁻¹²

Nowadays, a variety of coaxial rotor analysis methods exist ranging from low-fidelity methods to high-fidelity ones. In the following paragraphs, the highlights of each are presented.

At the low-fidelity end of the spectrum we have momentum theory, which assumes the rotor to be an infinitely thin disk through which there is an instantaneous pressure and velocity change that produces a thrust force. The main drawback of momentum theory is that it ignores the shape of the propeller (i.e. its aerodynamic characteristics), which obviously has a large impact on its behaviour and performance.⁶

A commonly used method is Blade Element Theory, which divides each rotor blade into a large number of elements along its radius where each element is represented as a 2-D airfoil with the assumption that there is no mutual effect between adjacent blade elements. An extension of BET is Blade Element Momentum Theory (BEMT) which, simply put, equals the lift calculated by the momentum theory with the lift from circulation theory used in the BET to estimate the inflow distribution along the blade. Leishman and Ananthan developed a more sophisticated mathematical model, based on BEMT, to predict the thrust and power of a coaxial-rotor in full size rotors.¹³

Another class of methods for predicting coaxial rotor performance are those based on panel methods.¹⁰ These methods are an extension of Prandtl's lifting-line theory, which uses the concept of circulation and the Kutta-Joukowski theorem. Within this category of methods several variations exist, such as the prescribed-wake model, in which a helical wake shape is iterated over to converge its pitch with the thrust produced by

the rotor, and Free-Wake Models (FVM), which are causal in nature but have to propagate vortex elements in the wake vortex sheet at each time-step, making them significantly more computationally expensive.

These methods are still several orders of magnitude faster than CFD methods such as Navier-Stokes equation solvers or the Lattice-Boltzmann Method (LBM) that is implemented in PowerFLOW®. These high-fidelity approaches rely on numerical methods requiring days to weeks to solve the flow around a specific coaxial rotor ([Figure 2](#)). Moreover, CFD method requires generation of grids, which is an entire challenge on its own.

2. Acoustic analogies for coaxial rotors

Two different analogies were considered for the aeroacoustic model, both compatible with unsteady loading cases on a coaxial rotor. The first is Ffowcs-Williams and Hawkings' aeroacoustic formulation^{[14](#)} in the time domain (source time). The original formulation can be implemented numerically using the Farassat-1A formulation in which the source time derivatives are transformed to observer time derivatives. The monopole and quadrupole terms for thickness and vortex noise, respectively, were not in the scope of the tool implemented, and instead the focus was put on modelling loading noise (dipole term).

Another technique that considers counter-rotating dipoles is the semi-analytical model proposed by Hanson.^{[15](#)} It predicts the far-field acoustic pressure for any CROR using the dipole source distribution over the blades.

In summary, analytical aeroacoustic methods are far behind those for single rotors, mainly due to the increased flow complexity, and the Blade-Vortex Interaction (BVI) noise emanating from the interaction of the wake of the top rotor with the lower rotor. These effects are amplified in non-axial flow conditions where the asymmetric flow conditions between the advancing and retreating sides of the disk combined with a skewed wake, result in unsteady loading on the blades of both rotors. At the same time, these non-axial flow conditions are very common in the urban air vehicle concepts such as the ones shown in [Figure 1](#).

One of the first steps in developing an acoustic conceptual design optimization tool for these type of vehicles is thus developing an analytical aeroacoustic model of coaxial rotors in non-axial, non-uniform inflow conditions and is precisely the goal of this work.

For reasons of speed and ease of implementation, a coupling between a modified BEMT formulation for coaxial rotors and Hanson's semi-analytical formulation was chosen for the aeroacoustic assessment tool presented in this paper.

The paper is structured as follows: **II.** Method describes the modelling approach of the developed aeroacoustic tool, **III.** Results & Discussion presents the predictions made by the aeroacoustic model and compares them, where possible, to experimental data. Finally, **IV.** Conclusion & Recommendations provides some concluding remarks and recommendations for the further development of this tool.

II. Method

The chronological approach of this project can be divided into 4 steps:

1. Implementation of Blade Element Momentum Theory (BEMT) for coaxial rotors in hover and axial flight based on the theory developed in.^{[13](#)}
2. Extension of BEMT to forward flight (non-axial flow), with skewed, contracted and non-uniform inflows and wakes.

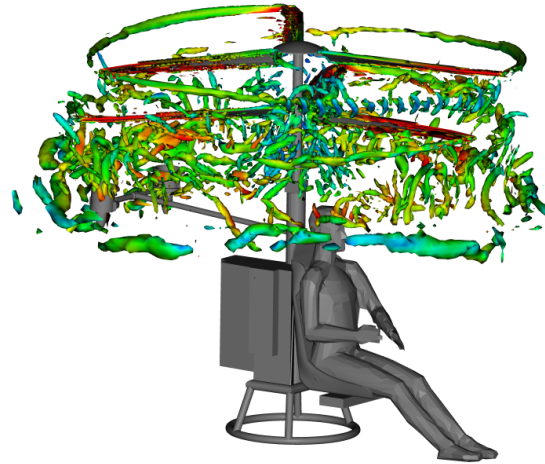


Figure 2: PowerFLOW®CFD simulation of Talaria's coaxial rotor system. Computations took around 18 hours on a computer cluster.

3. Extraction of blade element force vector time series.
4. Implementation of aeroacoustic analogy to compute far-field loading noise (harmonic noise component).

A. Aerodynamic Model: Extended BEMT for Coaxial Rotors

BEMT is a standard method for the analysis of helicopter rotors, it was formalized for coaxial rotors by Leishman in [3]. The advantage of BEMT is that it is based on solid physical principles (mass, momentum, and energy conservation laws, and the circulatory theory of lift) and is relatively free of empirical parameters. The theory discretizes the rotor disk into rotor annuli (concentric circles with small thickness) and applies momentum theory to each.

The main assumption of BEMT is that successive blade elements have no mutual effects on each other, (a two-dimensional assumption). Classic Prandtl “tip loss” effects have been included into the BEMT, giving a first approximation of the three-dimensional effects that occur due to tip and root vortices.

The theory developed Leishman additionally assumes the following:

- Small angle of attack. No high angle of attack corrections (linear lift polar and quadratic drag polar as best fits to XFOIL¹⁶ airfoil data).
- Limited to a rotor in hover or axial flight (cannot model the effects of a tangential flow component).
- Limited to positive pitch angles everywhere on the rotor disk.
- Small inflow angle. This is used to obtain closed-form solutions which give the method its tremendous speed advantage.
- The lower rotor does not produce induced interference at the upper rotor. This is a reasonable assumption for rotors with sufficient vertical separation.

The mathematical model for hover and axial flight was numerically implemented in MATLAB® and is robust to any rotor geometry. After successfully implementing an existing theory for hover and axial flight for both single and coaxial rotors the more challenging flight condition of forward flight was tackled. This represents the novel contribution of this work.

In forward flight, there is a lift asymmetry which means that thrust coefficients and inflow ratios will not only be a function of radius but also of azimuth angle (as clearly visible in Figure 4). Therefore, the rotor disk was discretized into disk elements instead of rotor annuli (as shown in Figure 3). A complete derivation of the novel forward flight BEMT formulation is given in Appendix Section B, only the main results are shown below:

$$\lambda(r, \psi) = \sqrt{\left(\frac{\sigma_u C_{l_\alpha}}{16Fr} \frac{\epsilon + r^2}{r + \lambda_T \sin \psi} - \frac{\lambda_P}{2}\right)^2 + \frac{\sigma_u C_{l_\alpha}}{8Fr} (\theta - \alpha_0)(\epsilon + r^2)} - \left(\frac{\sigma_u C_{l_\alpha}}{16Fr} \frac{\epsilon + r^2}{r + \lambda_T \sin \psi} - \frac{\lambda_P}{2}\right). \quad (1)$$

$$F = \frac{2}{\pi} \cos^{-1}(\exp(-f)). \quad (2)$$

with $\epsilon(r, \psi) = \lambda_T^2 \sin^2 \psi + 2\lambda_T r \sin \psi$. After a short fixed-point iteration between the inflow ratio λ and the Prandtl tip-loss function F , with an initial guess of $F = 1$, the whole rotor disk (≈ 26000 cells) can be converged simultaneously. It should be noted that if the tangential (to the rotor) flow velocity $V_T = 0$, the closed-form expression for λ reduced to the one derived by Leishman.¹³

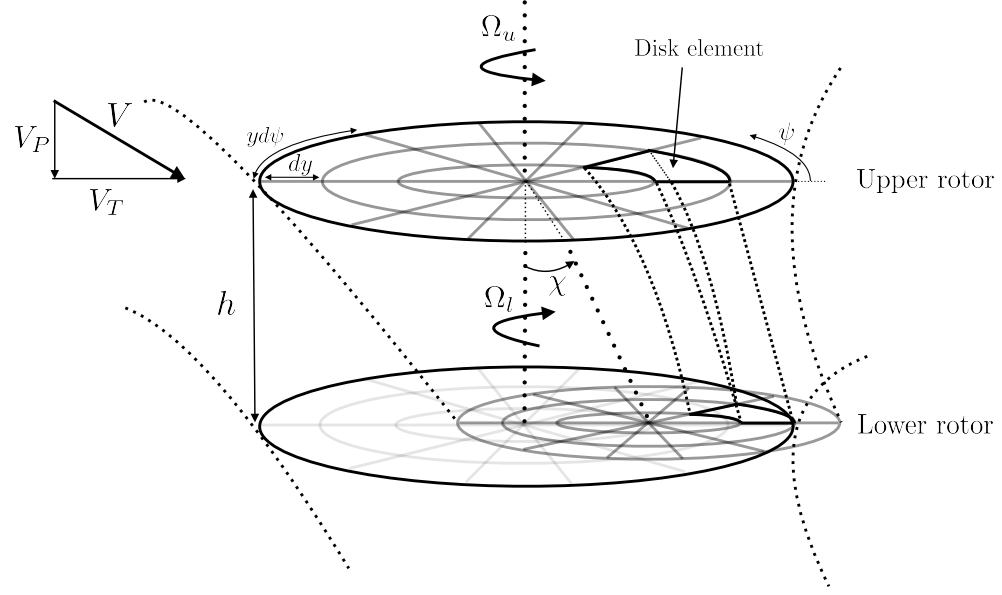
Next, we can use momentum theory to relate the thrust and power coefficients to the induced inflow at each disk element:

$$C_{T_u} = \int_0^{2\pi} \int_0^1 dC_{T_u} = \int_0^{2\pi} \int_0^1 \sigma_u \frac{C_{l_\alpha}}{2} (\theta - \phi - \alpha_0) (\lambda_T^2 \sin^2 \psi + 2\lambda_T r \sin \psi + r^2) dr \frac{d\psi}{2\pi} \quad (3)$$

$$C_{P_u} = \int_0^{2\pi} \int_0^1 dC_{Q_{u_i}} + dC_{Q_{u_p}} = \int_0^{2\pi} \int_0^1 \left(\frac{2}{\pi} \lambda^2 (\lambda - \lambda_P) + \sigma_u \frac{C_d}{4\pi} (\epsilon + r^2) \right) r dr d\psi. \quad (4)$$

Once the top rotor has been converged, the downwash is convected downstream as illustrated in Figure 3. The accelerated flow (due to a wake contraction of $a = 0.82$) impinges on the lower rotor and is used as

the non-uniform inflow of the lower rotor. The same iteration as for the top rotor is performed to find the induced inflow across the bottom rotor and with it the thrust and power coefficients. Note that this approach allows to model an arbitrary inflow distribution over the rotor disk, such as for instance the non-uniform (and possibly time-varying) inflow caused by the interaction of the rotor with a lifting body or a fuselage.



(a) Skewed and contracted wake of the upper rotor impinges on the lower rotor in forward flight

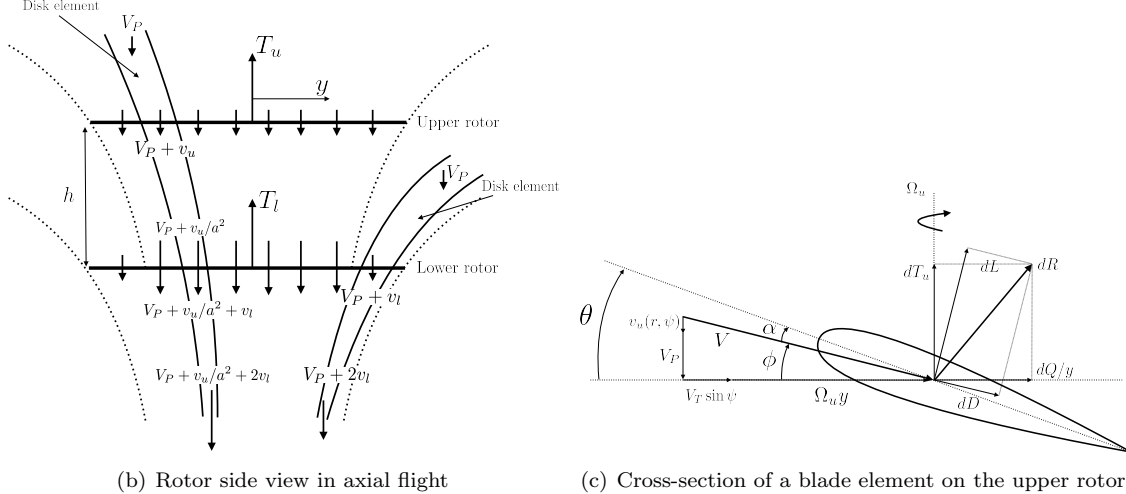


Figure 3: Extension of classical BEMT to coaxial rotors in forward flight. Both rotors are discretized in radial and azimuthal coordinates in the numerical implementation.

B. Acoustic Model: Hanson's Formulation for Coaxial Rotors

Once the lift and drag distributions have been found across the rotor, the force vector time-series on each blade element can be extracted by using the equality $C_l(r, \psi) = C_l(r, \Omega t)$ (analogously for C_d). Sample time-series are shown in [Figure 5](#) at different radial stations. The Fourier components of these loading terms (C_{lk} and C_{dk} , where $k = 0$ indicates the steady loading coefficient) can be used in Hanson's far-field formulation

to compute the unsteady loading noise characteristic of coaxial rotor configurations. The formulation for the general case, which deals with loading caused by the interaction between rotors of differing blade numbers and rotational speeds, is presented below. It should be noted that chordwise interference effects have been neglected (compact chord assumption), and offset and sweep phase delays have been removed from the original theory from Hanson.¹⁵

$$p(t) = \frac{-i\rho a_\infty^2 B_l \sin(\theta_o) R}{4\pi(d_o \sin(\theta_o))(1 - M_P \cos(\theta_o))} \sum_{m=-\infty}^{\infty} \sum_{k=-\infty}^{\infty} \exp\left\{i\left[(mB_l - kB_u)\left(\psi_o - \frac{\pi}{2}\right) + (mB_l\Omega_l + kB_u\Omega_u)\left(\frac{d_o}{a_\infty} - t\right)\right]\right\} \\ \times \int_0^{2\pi} \int_0^1 M J_{mB_l - kB_u} \left[\frac{(mB_l + kB_u\Omega_{ul})rM_T \sin(\theta_o)}{1 - M_P \cos(\theta_o)} \right] \left[k_x \frac{C_{dk}}{2} + k_y \frac{C_{lk}}{2} \right] dr d\psi \quad (5)$$

where

$$k_x = \frac{2M_T}{M} \left[\frac{mB_l + kB_u\Omega_{ul}}{1 - M_P \cos(\theta_o)} - kB_u(1 + \Omega_{ul}) \right] B_D \quad (6)$$

$$k_y = -\frac{2}{M} \left[\frac{(mB_l + kB_u\Omega_{ul})M_T^2 r \cos(\theta_o)}{1 - M_P \cos(\theta_o)} - \frac{(mB_l - kB_u)M_P}{r} \right] B_D \quad (7)$$

$$M = \sqrt{M_P^2 + ((\Omega r + V_T \sin(\psi))/a_\infty)^2} \quad (8)$$

and Ω_{ul} is the ratio of the two rotor speeds Ω_u/Ω_l and $M_T = (\Omega R + V_T)/a_\infty$, which have been adapted to include the free-stream tangential flow component.

The waveform formula above is computed for each rotor and superimposed to yield a resulting acoustic pressure history, from which an effective sound pressure and a sound pressure level through the following expressions.

$$p_{\text{RMS}} = \left[\frac{1}{T} \int_0^T p(t)^2 \right]^{1/2} \quad (9)$$

and

$$SPL = 20 \log_{10} \left[\frac{p_{\text{RMS}}}{p_{\text{ref}}} \right] \quad (10)$$

where T is the period of the acoustic signal, p_{RMS} is the Root-Mean-Square of the signal, p_{ref} is the reference sound pressure typically set to 2×10^{-5} Pa and SPL is the Sound Pressure Level in dB.¹⁷

III. Results & Discussion

This section showcases some results that are output by the developed tool for an example input. Consequently, the validation of the model in all flight phases is presented.

A. Sample tool output

The MATLAB® tool was run with the input parameters shown in Table 1. Some of the outputs of the tool are shown in Figure 4 and Figure 5 below and belong to the same case.

V_P [m/s]	10	Cyclic Input [-]	0	$\Omega_u = \Omega_l$ [rad/s]	40	ψ_o [deg]	0
V_T [m/s]	10	$\theta_u = \theta_l$ [deg]	20	θ_o [deg]	90	r_o [m]	150

Table 1: Input parameters for a test run of the implemented aeroacoustic tool. Note that the rotor used is the Harrington 1, the specifications of which are listed in Table 2

Figure 4 shows the distribution of angle of attack α , thrust and power coefficients dC_T and dC_P , inflow ratio λ , Prandtl tip-loss function F and inflow angle ϕ for both the upper and the lower rotor. By looking at the upper rotor, the influence of the tangential flow component is visible by noticing the advancing and retreating sides on the rotor disk. The white region in the α plots are regions where there is a negative angle

of attack (which will produce negative thrust in most cases) or where there is backflow. Momentum theory cannot model these two cases, which translates to a limitation of the current BEMT. Looking at the lower rotor plots, the impinging wake from the upper rotor is also discernible as a skewed and contracted elliptical shape).

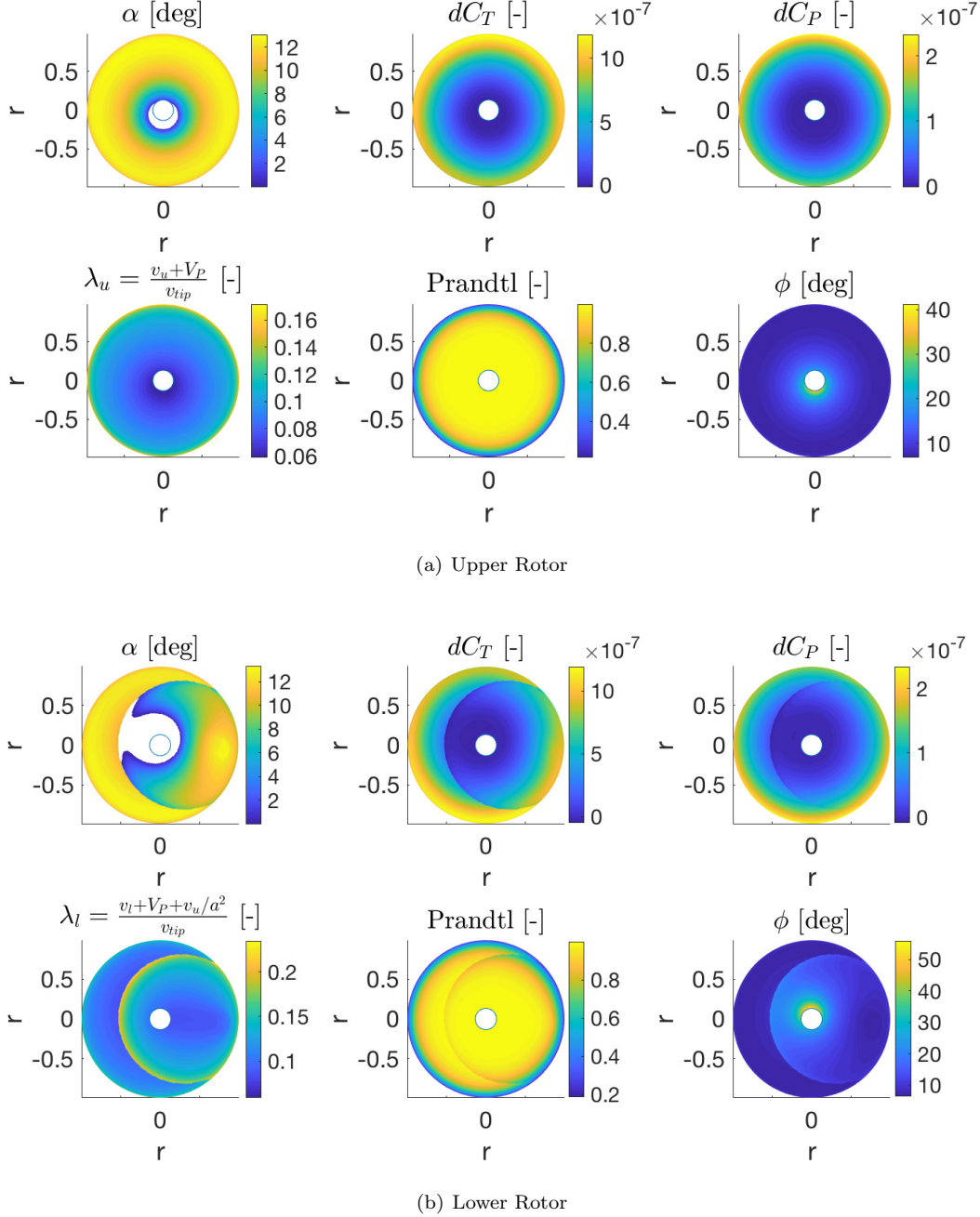
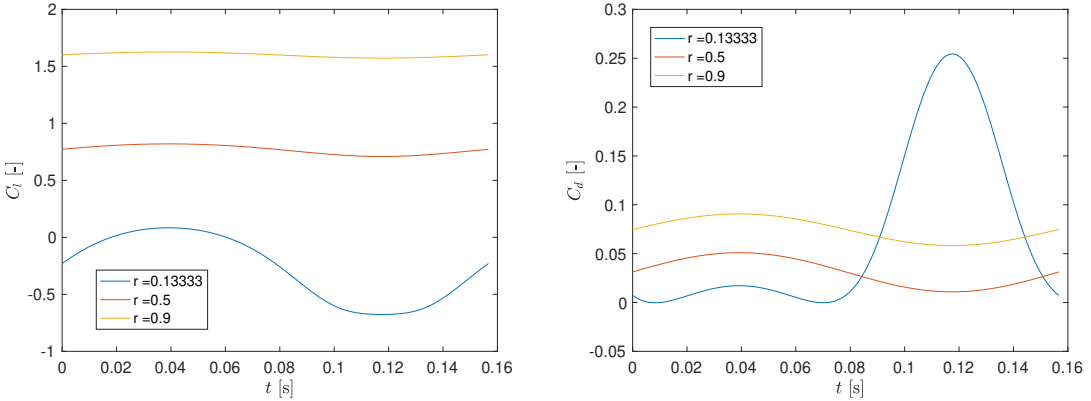
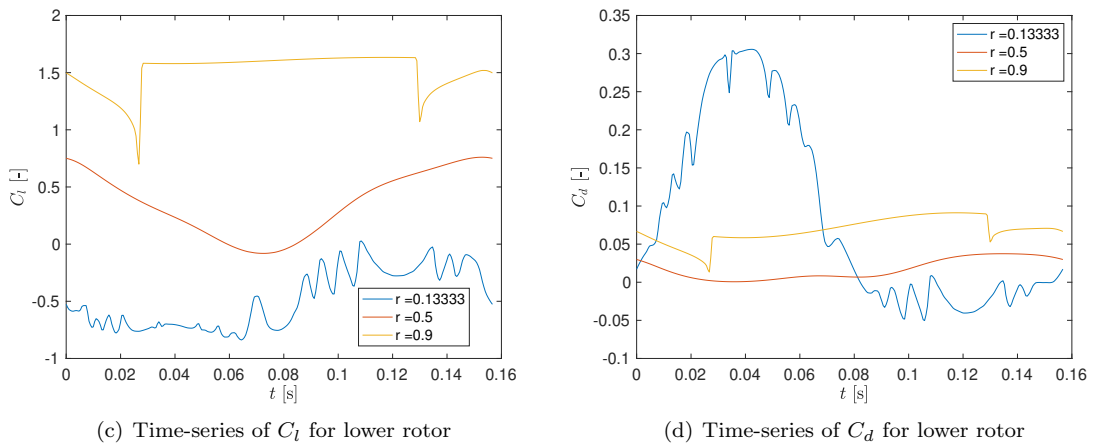
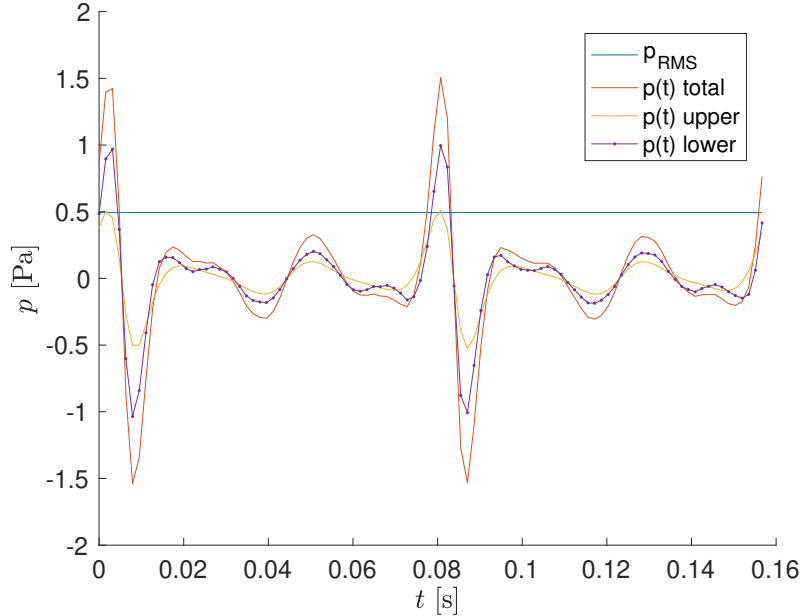


Figure 4: Sample output of the BEMT for the Harrington rotor 1 under the conditions specified in [Table 1](#) with the tangential flow component coming from the left. The top rotor rotates counter-clockwise and the lower rotor rotates clockwise. 26000 cells were converged in 0.17 seconds on a laptop.

(a) Time-series of C_l for upper rotor(b) Time-series of C_d for upper rotor(c) Time-series of C_l for lower rotor(d) Time-series of C_d for lower rotor

(e) Acoustic pressure time-series for upper and lower rotors and the effective acoustic pressure which is the Root-Mean-Square (RMS) of their superposition.

Figure 5: Fluctuation of loading coefficients (at different radial stations r) and acoustic pressure during one full rotation around the rotor disk.

By examining $dC_T(r, \psi)$ and $dC_P(r, \psi)$ for fixed values of r , a time-history of thrust and power coefficients as the blades spin around the upper and lower rotors can be obtained. Using the known distribution of inflow angles ϕ and the geometrical relations inferred from 3(c) presented in [Equation 13](#) and [Equation 14](#), the conversion to lift and drag coefficients can be made. For this particular case, such time-series are shown in [Figure 5](#). Note the drastic difference between the frequency of fluctuations for the upper rotor versus the lower rotor. Finally, using a Fast-Fourier-Transform (FFT), the loading harmonics (including the steady loading coefficients) can be found and passed to Hanson's formulation which, amongst other things, will calculate the acoustic pressure fluctuations emanating from the upper and lower rotors (see 5(e)). For this test case, with a discretization in time of 100 points, a discretization in ψ of 130 elements, in r of 100 elements, with 20 predominant loading and sound harmonics k and m these fluctuations result in a sound pressure level of 87.8 dB after a code convergence of 4.5 seconds on a laptop (0.2s for the BEMT and 4.3s for the acoustics).

B. Model Validation

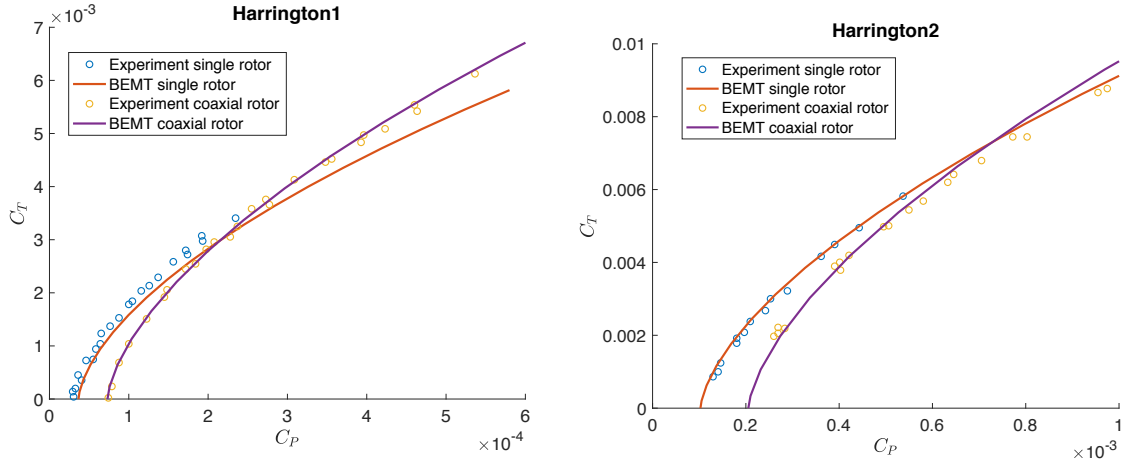
The BEMT aerodynamic performance model was validated in all flight conditions (hover, axial flight, forward flight) against a variety of coaxial and single rotors tested in wind-tunnel experiments. These rotors and their parameters (for reproducibility) are shown in [Table 2](#). As explained in [subsection B](#) a quadratic drag polar is used such that $C_d = C_{d_0} + D_1\alpha + D_2\alpha^2$ is a best fit to XFOIL¹⁶ data.

		Harrington 1	Harrington 2	NACA high-speed propeller	NACA coaxial propeller
General Parameters	Configuration	Single/Coaxial	Single/Coaxial	Single	Coaxial
	Inter-rotor spacing (h/R) [-]	0.186	0.16	-	0.5633
	Blade number [-]	2	2	3	3
	Rotor radius [m]	3.81	3.81	1.49	1.52
	Solidity per rotor [-]	0.027	0.076	0.23	0.078
	Hub radial fraction (y_{hub}/R) [-]	0.13	0.2	0.1	0.2
	Blade twist	Untwisted	Untwisted	Untwisted	Untwisted
Airfoil Parameters	Type	NACA 0012	NACA 0012	NACA 16006	Clark Y
	C_{l_α} [1/rad]	5.73	5.73	6.7	6.1
	α_0 [deg]	0	0	0	-3.75
	C_{d_0} [-]	0.011	0.011	0.003	0.007
	D_1 [1/rad]	0	0	0	0
	D_2 [1/rad ²]	1	1	3	0.8

Table 2: Rotors used for validation studies and their specifications. Data retrieved from Harrington⁹ for the Harrington 1 and 2 rotors, Evans¹⁸ for the NACA high-speed propeller and Biermann¹⁹ for the NACA coaxial propeller.

C. Hover

The Harrington rotors 1 and 2 (single and coaxial) were used as validation cases in hovering flight. Measurements of thrust and power are compared in [Figure 6](#). The predictions from the BEMT are very good in this regime and, notably, quite sensitive to airfoil lift and drag polars used (coefficients $C_{l_\alpha}, C_{d_0}, D_2$ in [Table 2](#)).



(a) Harrington 1 single and coaxial rotor, $V_{tip} = 152.4$ m/s. (b) Harrington 2 single and coaxial rotor, $V_{tip} = 109.5$ m/s

Figure 6: Validation of the BEMT for single and coaxial hovering rotors against measurements of thrust and power. Measurements for Harrington rotor 1 and 2 (results obtained at a torque balance). Curves obtained by progressively increasing the blade pitch.

There are almost no measured spanwise loading on coaxial rotors, therefore, the spanwise airloads predicted by a Free-Vortex Method (FVM) developed at the University of Maryland¹⁰ were compared to the predictions made by the BEMT. The agreement is acceptable in most cases in both magnitude and shape. The most noticeable differences occur near the root of the blade, where induced velocities are under-predicted and power is over-predicted by the BEMT. One possible cause of the former was thought to be the fact that the BEMT did not include Prandtl root vortex corrections. However, these corrections had only a very local, non-significant impact. Other discrepancies can be attributed to the fact that BEMT assumes that there is no mutual interaction between adjacent blade elements (despite the addition of the Prandtl tip correction function) whilst the FVM gives three-dimensional flow field predictions. It should also be kept in mind that this only serves as a verification, since the FVM is in itself just a prediction which might also have discrepancies with reality.

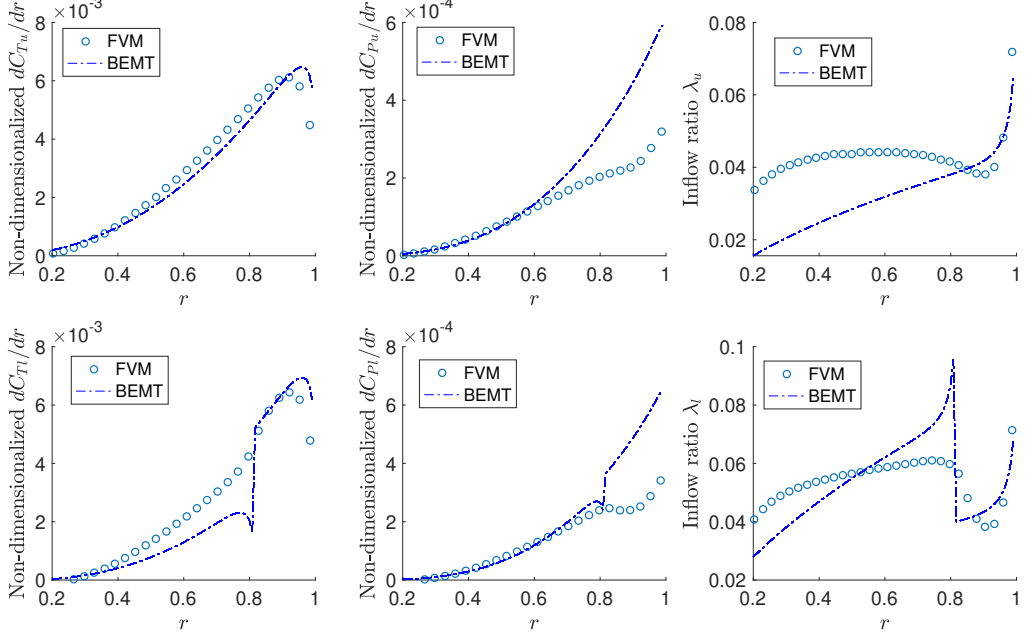
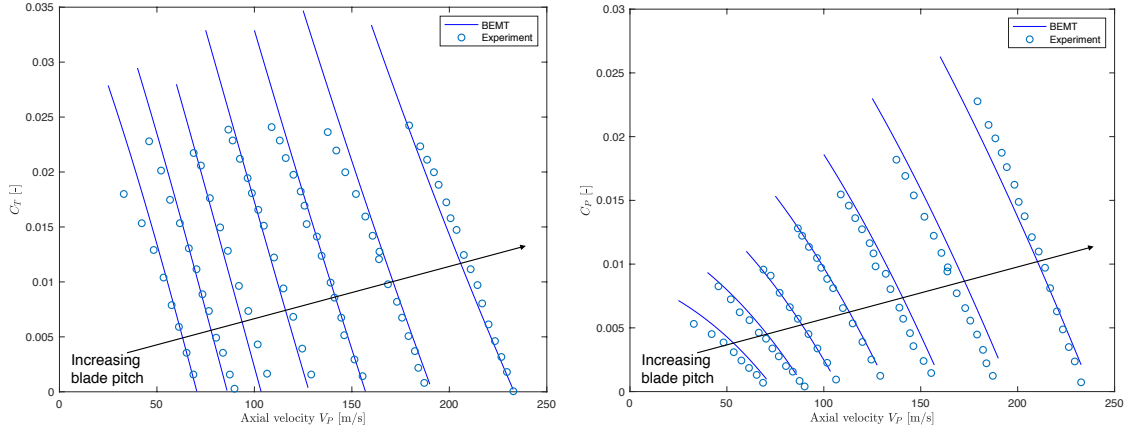


Figure 7: Predicted spanwise distribution of inflow, thrust and power coefficient for the upper and lower rotors using the BEMT and a Free-Vortex-Model (FVM). Results for Harrington rotor 1, $C_T = 0.004$ and $V_{tip} = 152.4$ m/s (results obtained at a torque balance).

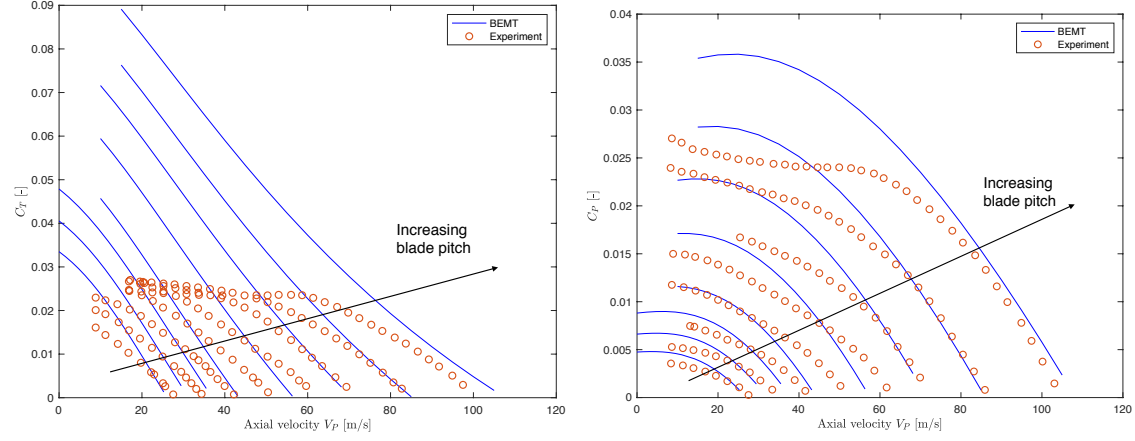
D. Axial Flight

The operating condition of axial flight was also validated with both single and coaxial rotors. The single rotor used was the NACA high-speed propeller (specifications shown in [Table 2](#)) which was tested up to helical tip Mach numbers of 1. Despite this, the agreement between the BEMT predicted power and thrust and the experimental data is remarkably good as can be seen in [8\(a\)](#) and [8\(b\)](#).

The contra-rotating rotor case is obviously more difficult than the single rotor case as the performance of both rotors has to be simultaneously predicted correctly. Not only that but the induced slipstream effects of the upper rotor on the lower rotor have to be accurately predicted. Compared to the NACA high-speed single propeller experiment, the coaxial rotors were tested on a wider range of velocities for a given pitch angle, thereby exposing them to deep stall conditions, which by looking at [8\(c\)](#) the BEMT did not handle very well (the thrust is significantly over-predicted, due to the linear aerodynamics in the model). The agreement in nominal regimes is almost as good as the agreement with the single rotor.



(a) Thrust predictions for the NACA single propeller at $V_{tip} = 249$ m/s (b) Power predictions for the NACA single propeller at $V_{tip} = 249$ m/s



(c) Thrust predictions for the NACA coaxial propeller at $V_{tip} = 87.5$ m/s (d) Power predictions for the NACA coaxial propeller at $V_{tip} = 87.5$ m/s

Figure 8: Validation of the BEMT with thrust and power measurements on a NACA high-speed propeller 8(a),8(b) and a NACA coaxial propeller 8(c),8(d) as a function of forward speed ratio (axial flight).

E. Forward Flight

Finally, the most challenging flight condition was tackled. Only one experiment was found in literature of a coaxial rotor (the Harrington 1) tested in non-axial flow conditions. This flight condition posed unique challenges to the theory developed since its main assumptions (such as small inflow and angle of attack angles) were questioned severely (especially on the retreating side of the rotors and the regions receiving the impinging wake from the upper rotor on the lower rotor). From Figure 9 it can be seen that the main physics of the coaxial rotor in forward flight are captured but not too accurately, especially in the mid-range of advance ratios μ . The over-prediction of power in these regimes might be attributed to the fact that the regions of back-flow show power coefficients of 0 in the BEMT while in reality they have slightly negative power coefficients. Another limitation might lie in the skewed wake model (which currently only uses convection of the induced velocity of individual disk elements). More sophisticated inflow models have been developed,²⁰ such as the one by Pitt-Peters, which take into account additional effects in forward flight such as that of increased inflow (clean air) at the front rotor side and reduced inflow at the back.

IV. Conclusion & Recommendations

A. Conclusion

A semi-analytical aeroacoustics tool was developed from an extended formulation of BEMT to model the performance of a coaxial rotor in forward flight, and a modified acoustic analogy based on Hanson's formulation. The performance predictions (from the BEMT) have been validated in hover, axial flight and forward flight for 6 different single and coaxial rotors and the accuracy is satisfactory for concept-level design and control applications (the model is being used in the flight controls of Talaria's Hermes II coaxial device). Due to a lack of acoustic measurements of coaxial rotors in forward flight, the integrated aeroacoustics tool has not been validated.

In optimization or control applications (the ultimate use case of this tool) it is not always the accuracy of the solution that matters but the robustness to large design spaces and operating conditions, the continuity and stability of the solutions and the speed of solution. With a model practically free of empirical parameters, and the results shown previously, it can be concluded that the predominant physics of coaxial rotor systems has been captured in this model at run times of ≈ 4.5 seconds for the combined aerodynamic and acoustic codes.

B. Recommendations

As mentioned previously, there currently exists scarce experimental data on the acoustic footprint of coaxial rotors (especially in forward flight). This fall, these types of experiments are planned by the Aeroacoustics group of the Faculty, as well as by the Talaria student team on their full-scale coaxial prototype. Hopefully this data can be used to validate the implementation of the acoustic part of the tool.

There is significant room for improvement both in modelling the aerodynamics as well as the acoustics of the coaxial rotor:

- Currently, the only empirical parameter in the entire aeroacoustic model is the contraction ratio of the upper rotor wake. A method by Landgrebe²¹ could be added to compute the contraction ratio as a function of the operating conditions of the coaxial.
- Different types of inflow models should be investigated. As mentioned previously in Section E, Pitt-Peter's model could model additional effects in forward flight. Another suitable addition to the model could be the method developed by Castles²² which calculates a field of induced velocities around a given rotor. In doing so, the induced interference produced at the upper rotor by the lower rotor could be captured.
- A revision of Hanson's aeroacoustic analogy (which had to be modified to account for tangential flow) or the implementation of Farassat's 1A formulation (possibly including source terms other than dipoles) would give confidence in the accuracy of the acoustic predictions made by the tool.
- Unsteady aerodynamic effects should be investigated. This might currently be a source of acoustic footprint over-prediction, since high-frequency loading harmonics are over-predicted. In reality, the aerodynamic response of a rotating airfoil will have delays which will remove the high-frequency components visible in 5(c) and 5(d).
- Finally, the robustness of the trim methods that were developed (gradient based) for the validation plots has to be improved such that different methods such as the one presented in Method 2 or the ones suggested above can be converged in the required operating conditions.

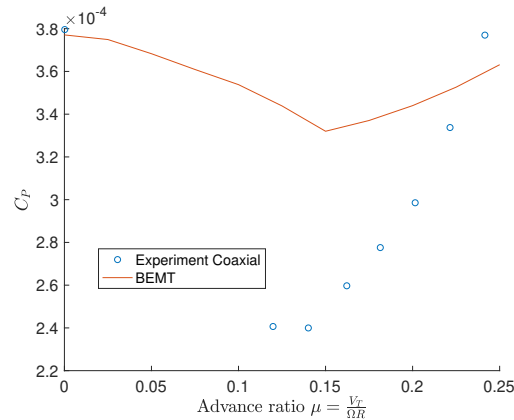


Figure 9: Comparison between extended BEMT predictions in forward flight and experimental data for the Harrington 1. Coaxial rotor trimmed at $C_T = 0.004$ with $V_{tip} = 142.95$ m/s

physics of coaxial rotor systems has been captured in this model at run times of ≈ 4.5 seconds for the combined aerodynamic and acoustic codes.

These additions and their possible benefits should, however, always be weighted against the computational burden they impose in order to maintain the unique advantage of this method: the fast solving speed.

If the tool is to be used now, in its most simple form, it could be used in a genetic algorithm to optimize top-level parameters such as blade number, blade twist, chord, taper, airfoil, rotor vertical spacing, etc, for minimum noise footprint in normal operation. Adding a second objective such as propulsive efficiency is also standard in genetic algorithms and can be done with the BEMT which is embedded in the aeroacoustics tool.

Acknowledgements

I would like to thank Daniele Ragni for supervising my research and providing valuable feedback. I would also like to thank Damiano Casalino, Edoardo Grande and Francesco Avallone for the helpful discussions. Lastly, I would like to acknowledge the Honours Programme Bachelor of the Delft University of Technology, for providing me with the unique opportunity to conduct this research.

References

- ¹Brown, A. and Harris, W., *A Vehicle Design and Optimization Model for On-Demand Aviation*, AIAA SciTech Forum, American Institute of Aeronautics and Astronautics, Jan 2018.
- ²Holden, J. and Goel, N., "UBER Elevate: Fast-Forwarding to a Future of On-Demand Urban Air Transportation," 2016, White Paper, Uber.
- ³Moore, M. D., "Concept of Operations for Highly Autonomous Electric Zip Aviation," *14th AIAA Aviation Technology and Integration and Operations (ATIO) Conference*.
- ⁴Kim, H. W. and Brown, R. E., "A Comparison of Coaxial and Conventional Rotor Performance," *Journal of the Helicopter Society*, Vol. 55, 2010.
- ⁵Prior, S. D., "Reviewing and Investigating the Use of Co-Axial Rotor Systems in Small UAVs," *International Journal of Micro Air Vehicles*, Vol. 2, No. 1, 2010.
- ⁶Tsadok, T., "Thruster Modeling for Small Unmanned Aerial Vehicles with Coaxial- Rotors," 2014, M. S. thesis, Dept. Mechanical Engineering, McGill Univ., Canada.
- ⁷Leishman, J. G. and Ananthan, S., "Aerodynamic Optimization of a Coaxial Proprotor," *Annual Forum Proceedings - AHS International*, 2006, pp. 64–86.
- ⁸Rankine, W. J. M., "On the Mechanical Principles of the Action of Propellers," .
- ⁹Harrington, R. D., "Full-Scale-Tunnel Investigation of the Static-Thrust Performance of a Coaxial Helicopter Rotors," *National Advisory Committee for Aeronautics*, 1951.
- ¹⁰Bagai, A. and Leishman, J. G., "Free-Wake Analysis of Tandem, Tilt-Rotor and Coaxial Rotor Configurations," *Journal of the American Helicopter Society*, Vol. 41, No. 3, 1996, pp. 196–207.
- ¹¹Leishman, J. G. and Syal, M., "Figure of Merit Definition for Coaxial Rotors," *Journal of the American Helicopter Society*, Vol. 53, No. 3, 2008, pp. 290–300.
- ¹²Leishman, J. G., "Aerodynamic Performance Considerations in the Design of a Coaxial Proprotor," *Journal of the American Helicopter Society*, Vol. 54, No. 1, 2009.
- ¹³Leishman, J. G. and Ananthan, S., "An Optimum Coaxial Rotor System for Axial Flight," *Journal of the American Helicopter Society*, Vol. 53, No. 4, 2008, pp. 366–381.
- ¹⁴Williams, J. E. F. and Hawkings, D. L., "Sound Generated by Turbulence and Surfaces in Arbitrary Motion," *Philosophical Transactions of the Royal Society of London*, Vol. A264, No. 1151, 1969, pp. 321–342.
- ¹⁵Hanson, D. B., "Noise Counter-rotation Propellers," *Journal of Aircraft*, Vol. 22, No. 7, 1985, pp. 609–617.
- ¹⁶Drela, M., "Xfoil: An interactive program for the design and analysis of subsonic isolated airfoils," Retrieved from: <http://web.mit.edu/drela/Public/web/xfoil>.
- ¹⁷Fahy, F. and Thompson, D., *Fundamentals of Sound and Vibration*, 2nd ed., CRC Press, 2015.
- ¹⁸Evans, A. J. and Liner, G., "Wind Tunnel Investigation of the Aerodynamic Characteristics of a Full-Scale Supersonic-Type Three-Blade Propeller at Mach Numbers to 0.96," *NACA Report*, Vol. 1375, 1958.
- ¹⁹Biermann, D. and Hartman, E., "Wind-Tunnel Tests of Four- and Six-Bladed Single- and Dual Rotating Tractor Propellers," *NACA Report*, Vol. 747, 1940.
- ²⁰Chen, R. T. N., "A Survey of Nonuniform Inflow Models for Rotorcraft Flight Dynamics and Control Applications," *NASA Technical Memorandum*, Vol. 102219, 1989.
- ²¹Landgrebe, A. J., "The wake geometry of a hovering helicopter rotor and its influence on rotor performance," *28th AHS forum*, 1972.
- ²²Castles, W. and Durham, H. L., "Distribution of Normal Component of Induced Velocity in Lateral Plane of Lifting Rotor," *NACA Technical Note*, , No. 3841, 1956.
- ²³Leishman, G., *Principles of Helicopter Aerodynamics*, Cambridge University Press, 2006.
- ²⁴Viterna, L. A. and Corrigan, R. D., "Fixed pitch rotor performance of large horizontal axis wind turbines," *NASA Lewis Research Center*, Vol. 19233, No. 83, 1982, pp. 69–85.

V. Appendices

A. Circulatory theory of lift

Blade Element and Momentum Theory brings together momentum theory and the circulatory theory of lift. The circulatory theory of lift, applied to an airfoil such as the one shown in 3(c) holds the following equations:

$$dL = \frac{1}{2} \rho V^2 C_{lc} dy \quad (11)$$

$$dD = \frac{1}{2} \rho V^2 C_{dc} dy \quad (12)$$

$$dT = B(dL \cos \phi - dD \sin \phi) \frac{d\psi}{2\pi} \quad (13)$$

$$dQ = B(dL \sin \phi + dD \cos \phi) y \frac{d\psi}{2\pi} \quad (14)$$

where the forces and moments are expressed here incrementally and act on an infinitesimally small area of the rotor disk $dA = r dr d\psi$. These results are crucial to understand the derivation that follows in subsection B.

B. Derivation of Forward Flight BEMT Formulation

In forward flight there is a lift asymmetry which means that thrust coefficients and inflow ratios will not only be a function of radius but also of azimuth angle. It makes sense to therefore discretize the rotor into disk elements instead of rotor annuli.

Each disk element will have an area of $dA = r dr d\psi$. To each of these disk elements, we can apply the fundamental result of momentum theory, which will relate the incremental thrust of each disk element and the inflow ratio there:²³

$$dT_u = 2\rho(V_P + v_u)v_u dA = 2\rho(V_P + v_u)v_u y dy d\psi \quad (15)$$

$$dC_{T_u} = \frac{dT_u}{\rho(\pi R^2)(\Omega R)^2} = \frac{2\rho(V_P + v_u)v_u y dy d\psi}{\rho(\pi R^2)(\Omega R)^2} \quad (16)$$

using the non-dimensional variables $dr = \frac{dy}{R}$, $r = \frac{y}{R}$ and $\lambda = \lambda_P + \lambda_u = \frac{V_P + v_u}{\Omega R}$, we obtain:

$$dC_{T_u} = \frac{2}{\pi} F \lambda \lambda_u r dr d\psi \quad (17)$$

where F is the Prandtl tip loss function:

$$F = \frac{2}{\pi} \cos^{-1}(\exp(-f)). \quad (18)$$

where f is given by:

$$f = \frac{B}{2} \left(\frac{1-r}{r\phi} \right) \quad (19)$$

where B is the number of blades, and ϕ is the inflow angle, which is equal to (based on 3(c)):

$$\phi = \tan^{-1} \left(\frac{v_u + V_P}{\Omega y + V_T \sin \psi} \right) = \tan^{-1} \left(\frac{\lambda}{r + \lambda_T \sin \psi} \right) \quad (20)$$

$$\approx \frac{\lambda}{r + \lambda_T \sin \psi} \quad (21)$$

where the last step uses a **small angle assumption** ($\phi \ll 1$). $\lambda_T = \frac{V_T}{\Omega R}$ is the non-dimensionalized tangential flow ratio. Based on whether we decide to continue the derivation with Equation 21 or Equation 20 we will encounter two different approaches, which respectively are:

1. Solve for λ in closed-form as done in¹³ for the axial flight case. Only use non-dimensional variables.
2. Iterative process between dC_{T_u} , λ and F . dC_{T_u} is then calculated with no small angle assumptions.

1. *First approach*

If we assume that $\phi \ll 1$ (small angle assumption), then we can write [Equation 13](#) as:

$$dT_u = BdL \frac{d\psi}{2\pi} = B \frac{\rho}{2} C_l V^2 c dy \frac{d\psi}{2\pi} \quad (22)$$

where C_l and V can be expanded, respectively, as:

$$C_l = C_{l_\alpha}(\alpha - \alpha_0) = C_{l_\alpha}(\theta - \phi - \alpha_0) \quad (23)$$

$$V = V_T \sin \psi + \Omega y \quad (24)$$

which can be inferred from [3\(c\)](#) using small angle assumptions (ϕ is given by [Equation 21](#)). Writing [Equation 22](#) in non-dimensional form, we obtain:

$$\begin{aligned} dC_{T_u} &= \frac{Bc}{\pi R} \frac{C_{l_\alpha}}{2} (\theta - \phi - \alpha_0) \left(\frac{V_T^2 \sin^2 \psi}{(\Omega R)^2} + \frac{2V_T \sin \psi \Omega y}{(\Omega R)^2} + \frac{(\Omega y)^2}{(\Omega R)^2} \right) dr \frac{d\psi}{2\pi} \\ &= \sigma_u \frac{C_{l_\alpha}}{2} (\theta - \phi - \alpha_0) (\lambda_T^2 \sin^2 \psi + 2\lambda_T r \sin \psi + r^2) dr \frac{d\psi}{2\pi} \end{aligned} \quad (25)$$

where σ_u is the rotor solidity, by definition. Equating the above expression to the one previously found in [Equation 17](#), and defining $\epsilon(r, \psi) = \lambda_T^2 \sin^2 \psi + 2\lambda_T r \sin \psi$ for brevity, we obtain:

$$\sigma_u \frac{C_{l_\alpha}}{2} \left(\theta - \frac{\lambda}{r + \lambda_T \sin \psi} - \alpha_0 \right) (\epsilon + r^2) dr \frac{d\psi}{2\pi} = \frac{2}{\pi} F \lambda (\lambda - \lambda_P) r dr d\psi \quad (26)$$

$$\frac{\sigma_u C_{l_\alpha}}{8Fr} (\theta - \alpha_0) (\epsilon + r^2) - \frac{\sigma_u C_{l_\alpha}}{8Fr} \frac{\lambda}{r + \lambda_T \sin \psi} (\epsilon + r^2) = \lambda (\lambda - \lambda_P) \quad (27)$$

$$\lambda^2 + \left(\frac{\sigma_u C_{l_\alpha}}{8Fr} \frac{\epsilon + r^2}{r + \lambda_T \sin \psi} - \lambda_P \right) \lambda - \frac{\sigma_u C_{l_\alpha}}{8Fr} (\theta - \alpha_0) (\epsilon + r^2) = 0 \quad (28)$$

$$\lambda(r, \psi) = \sqrt{\left(\frac{\sigma_u C_{l_\alpha}}{16Fr} \frac{\epsilon + r^2}{r + \lambda_T \sin \psi} - \frac{\lambda_P}{2} \right)^2 + \frac{\sigma_u C_{l_\alpha}}{8Fr} (\theta - \alpha_0) (\epsilon + r^2) - \left(\frac{\sigma_u C_{l_\alpha}}{16Fr} \frac{\epsilon + r^2}{r + \lambda_T \sin \psi} - \frac{\lambda_P}{2} \right)}. \quad (29)$$

Note that [Equation 29](#) reduces to the expression derived in¹³ in axial flight ($\lambda_T = 0$). The same iteration is required between λ and F .

Obtaining the incremental torque coefficient is straightforward having found λ and dC_{T_u} . By using a small angle assumption, we can find the profile and induced torque coefficients:

$$dC_{Q_{u_p}} = \frac{By \frac{d\psi}{2\pi} dD}{\rho(\pi R^3)(\Omega_u R)^2} = \frac{By \frac{d\psi}{2\pi} \frac{1}{2} \rho V^2 C_d c dy}{\rho(\pi R^3)(\Omega_u R)^2} = \frac{Bc}{\pi R} \frac{y}{R} \frac{dy}{R} \left(\frac{V}{\Omega R} \right)^2 \frac{C_d d\psi}{4\pi} = \sigma_u r dr d\psi \frac{C_d}{4\pi} (\epsilon + r^2). \quad (30)$$

$$dC_{Q_{u_i}} = \lambda dC_{T_u} = \frac{2}{\pi} \lambda^2 \lambda_u r dr d\psi = \frac{2}{\pi} \lambda^2 (\lambda - \lambda_P) r dr d\psi \quad (31)$$

Integrating the incremental thrust and torque coefficients over the disk yields:

$$C_{T_u} = \int_0^{2\pi} \int_0^1 dC_{T_u} = \int_0^{2\pi} \int_0^1 \sigma_u \frac{C_{l_\alpha}}{2} (\theta - \phi - \alpha_0) (\lambda_T^2 \sin^2 \psi + 2\lambda_T r \sin \psi + r^2) dr \frac{d\psi}{2\pi} \quad (32)$$

$$C_{P_u} = \int_0^{2\pi} \int_0^1 dC_{Q_{u_i}} + dC_{Q_{u_p}} = \int_0^{2\pi} \int_0^1 \left(\frac{2}{\pi} \lambda^2 (\lambda - \lambda_P) + \sigma_u \frac{C_d}{4\pi} (\epsilon + r^2) \right) r dr d\psi \quad (33)$$

Performing this for the lower rotor is very similar. The most important changes are:

- Change sign of $\sin \psi$ since the rotor rotates in the opposite direction.
- In [Equation 29](#), λ_P will be replaced by a function of r and ψ . This function will be equal to λ_P for the disk elements on the lower rotor that are unaffected by the downwash of the upper rotor. For the disk elements that are affected by the upper rotor downwash V_P will be replaced by $V_P + \lambda_{u_{\text{interp}}}/a^2$, where a is the radial contraction of the wake and $\lambda_{u_{\text{interp}}}$ is the interpolated inflow ratio on the mapped location of the lower rotor disk element on the upper rotor.

2. Second approach

F , λ_u and dC_{T_u} are functions of ψ and r . Now, one can start with a guess for each disk element of $F = 1$ (as recommended in [13](#)) and a guess for λ_u . Note that these guesses could come from running the second (fast) approach a few times. Then,

$$dC_{T_u} = \frac{B(dL \cos \phi - dD \sin \phi) \frac{d\psi}{2\pi}}{\rho(\pi R^2)(\Omega_u R)^2} = \frac{B \frac{1}{2} \rho V^2 c dy (C_l \cos \phi - C_d \sin \phi) \frac{d\psi}{2\pi}}{\rho(\pi R^2)(\Omega_u R)^2} \quad (34)$$

$$= \frac{B c dr}{2\pi R} ((\lambda_T \sin \psi + r)^2 + \lambda^2) (C_l \cos \phi - C_d \sin \phi) \frac{d\psi}{2\pi} \quad (35)$$

yields the incremental thrust coefficient of that disk element. Recall that ϕ in this equation is calculated exactly as done in [Equation 20](#). dL and dD are functions of the angle of attack of the blade at that disk element and can be calculated with tools like XFOIL or a look-up table. V is modified with respect to [Equation 24](#) and is now:

$$V = \sqrt{(V_T \sin \psi + \Omega_u y)^2 + (v_u + V_P)^2} \quad (36)$$

such that,

$$\frac{V^2}{(\Omega_u R)^2} = \frac{(V_T \sin \psi + \Omega_u y)^2 + (v_u + V_P)^2}{(\Omega_u R)^2} = (\lambda_T \sin \psi + r)^2 + \lambda^2 \quad (37)$$

Now, rearranging [Equation 17](#) into a quadratic equation, yields a solution for λ_u :

$$\lambda_u^2 + \lambda_P \lambda_u - \frac{\pi dC_{T_u}}{2 Fr dr d\psi} = 0 \quad (38)$$

$$\lambda_u = \sqrt{\left(\frac{\lambda_P}{2}\right)^2 + \frac{\pi dC_{T_u}}{2 Fr dr d\psi} - \frac{\lambda_P}{2}} \quad (39)$$

With the calculated λ_u we can recalculate ϕ . Subsequently, we can calculate F and dC_{T_u} , after which we can recalculate λ_u and the iteration continues.

The incremental torque coefficient can also be found using blade-element theory (i.e. the circulation theory of lift):

$$dC_{Q_u} = dC_{P_u} = \frac{B(dL \sin \phi + dD \cos \phi) y \frac{d\psi}{2\pi}}{\rho(\pi R^3)(\Omega_u R)^2} = \frac{B c dr}{2\pi R} ((\lambda_T \sin \psi + r)^2 + \lambda^2) (C_l \sin \phi + C_d \cos \phi) \frac{d\psi}{2\pi} \quad (40)$$

An early empirical model by Viterna²⁴ was used to correct airfoil properties beyond stall.

For $\alpha > \alpha_s$:

$$C_l = \frac{C_{d,\max}}{2} \sin 2\alpha + K_l \frac{\cos^2 \alpha}{\sin \alpha} \quad (41)$$

$$C_d = C_{d,\max} \sin^2 \alpha + K_d \cos \alpha \quad (42)$$

$$K_l = (C_{l,s} - C_{d,\max} \sin \alpha_s \cos \alpha_s) \frac{\sin \alpha_s}{\cos^2 \alpha_s} \quad (43)$$

$$K_d = \frac{C_{d,s} - C_{d,\max} \sin^2 \alpha_s}{\cos \alpha_s} \quad (44)$$

$$\frac{R}{c} \leq 50 : C_{d,\max} = 1.11 + 0.018 \frac{R}{c} \quad (45)$$

$$\frac{R}{c} > 50 : C_{d,\max} = 2.01 \quad (46)$$

where $C_{d,\max}$ is the maximum drag coefficient, α_s is the stall angle of attack, $C_{d,s}$ and $C_{l,s}$ are the drag and lift coefficients at $\alpha = \alpha_s$.